Dislocation and traction loads over an elliptical region in anisotropic magnetoelectroelastic bimaterials

2013 Smart Mater. Struct. 22 125020

(http://iopscience.iop.org/0964-1726/22/12/125020)

Smart Mater. Struct. **22** (2013) 125020 (14pp) doi:10.1088/0964-1726/22/12/125020

Dislocation and traction loads over an elliptical region in anisotropic magnetoelectroelastic bimaterials

Haijian Chu[1], **Huiming Wang**[2], **Yanfei Zhao**[3] **and Ernian Pan**[3]

[1] Department of Mechanics, College of Sciences, Shanghai University, Shanghai 200444, People's Republic of China
[2] Department of Engineering Mechanics, Zhejiang University, Hangzhou 310027, People's Republic of China
[3] Computer Modeling and Simulation Group, University of Akron, Akron, OH 44325, USA

E-mail: pan2@uakron.edu

Received 16 May 2013, in final form 17 September 2013
Published 14 November 2013
Online at stacks.iop.org/SMS/22/125020

Abstract
In indentation tests of material properties and in the analysis of the interaction between a structure and its foundation, the solution for a uniform loading over an elliptical area in a half-space is essential. Thus, in this paper, we derive the analytical solution for a general magnetoelectroelastic bimaterial system under the action of extended traction and dislocation uniformly distributed over a horizontal ellipse. The solution is obtained by making use of two-dimensional Fourier transformation combined with the Stroh formalism. To deal with the elliptical shape, a simple scale transformation technique is applied. As such, our solution is very general and contains various decoupled material systems and reduced material domains (infinite and half-space) as special cases. As numerical examples, a bimaterial system made of $BaTiO_3/CoFe_2O_4$ is studied under both traction and dislocation loads within the elliptical area with various semi-axes ratios. It is shown that the induced field due to traction is smoother than that due to dislocation and that both the elliptical semi-axes ratios and material orientation can significantly influence the induced elastic, electric and magnetic fields.

(Some figures may appear in colour only in the online journal)

1. Introduction

Due to their product property, composites made of piezoelectric and piezomagnetic materials can exhibit a special coupling between the electric and magnetic field effects through the mechanical strain interaction between the two dissimilar materials (Ryu *et al* 2002, Wang *et al* 2009). Such composites behave similarly to the new multiferroics in material sciences (Eerenstein *et al* 2006, Ma *et al* 2011).

Fundamental solutions, particularly the Green function solutions, are important for understanding the basic features associated with the multiferroics material system and for serving as the kernel functions for more complicated problems. Recently, various Green function solutions in magnetoelectroelastic (MEE) or multiferroic systems have been derived and reported in the literature. For example, Liu *et al* (2001) derived the Green functions in anisotropic MEE solids with an elliptical cavity or a crack. Ding *et al* (2005) obtained the Green functions for two-phase transversely isotropic MEE media. Wang and Pan (2008) found the time-dependent Green functions in anisotropic multiferroic bimaterials with a viscous interface subject to the extended line force and dislocation. Important progress in Green function solution was also reported for MEE materials subjected to loads over a circular region (Chu *et al* 2011, Wang *et al* 2012, Zhao *et al* 2013).

It is well known that in an indentation test of material properties, the contact area between the two materials is, in general, of an elliptical shape (e.g., Willis 1966). Similarly, the contact area between a structure and its foundation may, in general, be in an elliptical shape (Deresiewicz 1960). However, to the best knowledge of the authors, only in the paper by Deresiewicz (1960) has the response of the three-dimensional elastic half-space under elliptical loading been studied analytically. Thus, it is desirable to have an analytical solution of a three-dimensional magnetoelectroelastic (MEE) half or bimaterial system under a uniform loading over an elliptical area, which is the goal of this paper.

In this paper, after the introduction, we present, in section 2, the mathematical model for the MEE bimaterial system under an internal uniform load over a horizontal ellipse. In section 3, by combining the Fourier transform and Stroh theory, we derive the solutions in both the Fourier-transformed and physical domains in terms of double integrations. After scaling the elliptical region to a circular one, the method introduced in Zhao *et al* (2013) for the circular loading region is applied. In section 4, we obtain the physical-domain solutions in terms of a simple line integral from 0 to 2π. In section 5, numerical examples for $BaTiO_3/CoFeO_4$ bimaterials are given, and the influence of the shape of the ellipse and crystal orientation on the elastic field, electric displacement and magnetic induction is demonstrated. Conclusions are drawn in section 6. It should be pointed out that the present solution for the elliptical loading region is general and can be directly reduced to the one in Zhao *et al* (2013) as a special case. Furthermore, the solution obtained in this paper can be reduced easily to the elliptical loading solutions in the corresponding uncoupled material systems, including piezoelectric and purely elastic bimaterial or half-space.

2. Mathematical model

2.1. Fundamental formula for MEE material

Using the short notation introduced by Barnett and Lothe (1975), the extended equilibrium equations for MEE materials in terms of the extended stresses σ_{iJ} can be expressed as (Pan 2002)

$$\sigma_{iJ,i} + f_J = 0, \tag{1}$$

where f_J is the extended body force, and the repeated lowercase (uppercase) indices take the summation from 1 to 3 (or 1–5). An index following the subscript ', i' indicates the derivative with respect to the coordinate x_i.

The generalized and fully coupled constitutive equations in terms of the extended material coefficients c_{iJKl} have the following form (Zhao *et al* 2013):

$$\sigma_{iJ} = c_{iJKl} u_{K,l}. \tag{2}$$

Detailed definitions of the notation used here are given in appendix A. Substituting equation (2) into equation (1), we obtain the governing equations in terms of the extended displacements u_K for a homogeneous MEE material (the material coefficients c_{iJKl} are constant) in the form

$$c_{iJKl} u_{K,li} + f_J = 0. \tag{3}$$

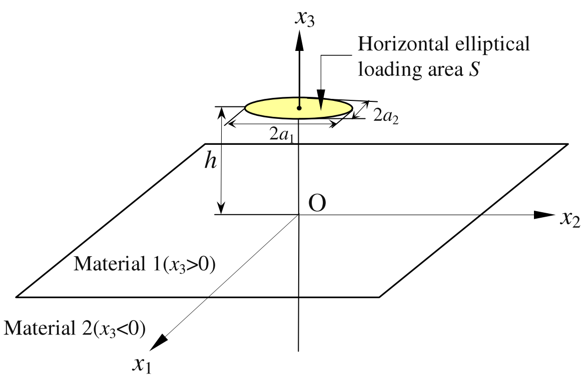

Figure 1. Sketch of an anisotropic MEE bimaterial space subject to a uniform extended traction or dislocation within an elliptical area of semi-axes a_1 and a_2 which is centered at $(x_1, x_2, x_3) = (0, 0, h)$.

It should be noted that the governing equations for the fully coupled MEE systems in equation (3) are exactly the same in mathematical form as their piezoelectric and purely elastic counterparts, except for the difference in the dimension of the involved quantities. This implies that the solution method developed in anisotropic elasticity can be directly applied to the anisotropic MEE case. On the other hand, once the general solution to the three-dimensional (3D) fully coupled MEE system is derived, we can reduce our solution to the 3D piezoelectric, piezomagnetic, and purely elastic cases by setting the corresponding coupling material constants to be zero. For example, reducing the uppercase index from 5 to 4 (as its upper limit) will give us the solutions to either the piezoelectric or piezomagnetic case. For the piezomagnetic case, the piezoelectric quantities associated with index 4 need to be replaced by the piezomagnetic quantities associated with index 5. For the anisotropic elastic case, all the indices are limited to 3.

2.2. Boundary value problem of MEE bimaterials

We consider a bimaterial system of general linear anisotropic MEE materials, as shown in figure 1. The upper ($x_3 > 0$) and lower ($x_3 < 0$) half-spaces are assigned as Materials 1 and 2, respectively. Within a horizontal elliptical area denoted by S in Material 1 at $x_3 = h (S \subset C : 1 - (x_1/a_1)^2 - (x_2/a_2)^2 = 0)$, either the 'extended' dislocation vector or 'extended' traction vector is applied. Here a_1 and a_2 are the major and minor radii (or semi-axes) of the ellipse, respectively. The goal of this paper is to derive the solutions of the elastic, electric, and magnetic fields due to the uniform extended dislocation and traction applied in the elliptical area.

In order to find the solution to this problem, the bimaterial infinite space is divided into three subdomains: $x_3 < 0$, $0 < x_3 < h$, and $x_3 > h$. Since there is no body source within any domain, namely the body force is zero, we have $f_J = 0$ in equation (3).

Solutions to equation (3) should satisfy the following conditions: (I) the extended displacement and traction in subdomains $x_3 < 0$ and $0 < x_3 < h$ should be continuous across the interface $x_3 = 0$; (II) the solution in subdomains

$0 < x_3 < h$ and $x_3 > h$ should satisfy the given discontinuity conditions at $x_3 = h$; (III) the solutions in the upper and lower half-spaces should approach zero when the field point $|\boldsymbol{x}| = \sqrt{x_1^2 + x_2^2 + x_3^2}$ approaches infinity. These conditions are presented below in equation form.

The interface of the two half-spaces is assumed to be perfect; namely the extended displacement vector $\boldsymbol{u} = (u_1, u_2, u_3, u_4, u_5)^{\mathrm{T}} \equiv (u_1, u_2, u_3, \phi, \psi)^{\mathrm{T}}$ and the extended traction vector $\boldsymbol{t} = (t_1, t_2, t_3, t_4, t_5)^{\mathrm{T}} = (t_1, t_2, t_3, D_3, B_3)^{\mathrm{T}}$ are required to satisfy the following continuity conditions across the interface $x_3 = 0$:

$$\begin{aligned} \boldsymbol{u}(x_1, x_2, 0^+) - \boldsymbol{u}(x_1, x_2, 0^-) &= \boldsymbol{0} \\ \boldsymbol{t}(x_1, x_2, 0^+) - \boldsymbol{t}(x_1, x_2, 0^-) &= \boldsymbol{0}. \end{aligned} \tag{4}$$

In the extended displacement vector $\boldsymbol{u}$ and extended traction vector $\boldsymbol{t}$, the ϕ, ψ, D_3 and B_3 are the electric potential, magnetic potential, electric displacement component in the x_3-direction and magnetic induction component in the x_3-direction, respectively.

On the horizontal plane $x_3 = h$ between the subdomains $0 < x_3 < h$ and $x_3 > h$ within the same material domain, the extended displacement and traction vectors should be continuous outside the loading area. However, within the loading area, the following discontinuity conditions should be satisfied.

For the case of applied extended dislocations, the extended displacement within the elliptical region S should satisfy

$$\begin{aligned} &u_J(x_1, x_2, h^+) - u_J(x_1, x_2, h^-) \\ &\quad \equiv d_J = \begin{cases} d_j & (J = 1, 2, 3) \\ \Delta\phi & (J = 4) \\ \Delta\psi & (J = 5), \end{cases} \end{aligned} \tag{5}$$

where the extended dislocations d_J are the given values which include the elastic ($J = j = 1, 2, 3$), electric ($J = 4$) and magnetic ($J = 5$) dislocations applied over the elliptical area S.

For the case of applied extended tractions, we should have, in the elliptical area,

$$\begin{aligned} &t_J(x_1, x_2, h^+) - t_J(x_1, x_2, h^-) \\ &\quad \equiv T_J = \begin{cases} T_j & (J = 1, 2, 3) \\ D_3 & (J = 4) \\ B_3 & (J = 5), \end{cases} \end{aligned} \tag{6}$$

where the extended tractions T_J are the given values which include the elastic traction ($J = j = 1, 2, 3$), normal electric displacement ($J = 4$) and normal magnetic induction ($J = 5$) applied over the elliptical area S.

In addition, since the extended displacements and stresses at infinity should be zero, we have

$$\lim_{|\boldsymbol{x}|\to\infty} u_J = 0, \qquad \lim_{|\boldsymbol{x}|\to\infty} \sigma_{iJ} = 0. \tag{7}$$

Thus, the boundary value problem is to solve the governing equation (3) with $f_J = 0$ in the three subdomains subject to conditions (4)–(7).

3. General solution

3.1. General solution in the Fourier-transformed domain

We define the two-dimensional Fourier transform as

$$\tilde{f}(k_1, k_2, x_3) = \iint f(x_1, x_2, x_3) \mathrm{e}^{\mathrm{i}(k_1 x_1 + k_2 x_2)}\, \mathrm{d}x_1\, \mathrm{d}x_2, \tag{8}$$

where k_1 and k_2 denote the variables in the Fourier-transformed domain corresponding to x_1 and x_2 in the physical domain, respectively. The corresponding Fourier inverse transform is

$$f(x_1, x_2, x_3) = \frac{1}{4\pi^2} \iint \tilde{f}(k_1, k_2, x_3) \mathrm{e}^{-\mathrm{i}(k_1 x_1 + k_2 x_2)}\, \mathrm{d}k_1\, \mathrm{d}k_2. \tag{9}$$

In the Fourier-transformed domain, the applied uniform extended traction at $x_3 = h$ becomes

$$\tilde{T}_J(k_1, k_2, h) = T_J \iint_S \mathrm{e}^{\mathrm{i}(k_1 x_1 + k_2 x_2)}\, \mathrm{d}x_1\, \mathrm{d}x_2. \tag{10}$$

To carry out the integral over the elliptical domain, we introduce a scale transformation $x_1/a_1 = y_1/R$, and $x_2/a_2 = y_2/R$ with $R = (a_1 a_2)^{1/2}$ so that equation (10) can be rewritten as

$$\tilde{T}_J(k_1, k_2, h) = T_J \iint_{S_R} \mathrm{e}^{\mathrm{i}(a_1 k_1 y_1 + a_2 k_2 y_2)/R}\, \mathrm{d}y_1\, \mathrm{d}y_2. \tag{11}$$

Obviously, the original elliptical integral domain S is transformed into a circle area $S_R(1 = (y_1/R)^2 + (y_2/R)^2)$, which could greatly simplify the derivation. Furthermore, we let $a_1 k_1/R = \lambda_1$ and $a_2 k_2/R = \lambda_2$, so that equation (11) becomes

$$\tilde{T}_J(\lambda_1, \lambda_2, x_3) = T_J \iint_{S_R} \mathrm{e}^{\mathrm{i}(\lambda_1 y_1 + \lambda_2 y_2)}\, \mathrm{d}y_1\, \mathrm{d}y_2. \tag{12}$$

Similarly, in the Fourier-transformed domain, the displacement jump condition for the applied uniform extended dislocation is

$$\tilde{d}_J(\lambda_1, \lambda_2, x_3) = d_J \iint_{S_R} \mathrm{e}^{\mathrm{i}(\lambda_1 y_1 + \lambda_2 y_2)}\, \mathrm{d}y_1\, \mathrm{d}y_2. \tag{13}$$

In summary, for a uniform load over the elliptic domain $S(1 = (x_1/a_1)^2 + (x_2/a_2)^2)$, or a uniform load over the transformed circular domain $S_R(1 = (y_1/R)^2 + (y_2/R)^2)$, equations (12) and (13) become

$$\begin{bmatrix} \tilde{\boldsymbol{d}} \\ \tilde{\boldsymbol{T}} \end{bmatrix} (\lambda_1, \lambda_2, x_3) = 2\pi R \frac{J_1(\eta R)}{\eta} \begin{bmatrix} \boldsymbol{d} \\ \boldsymbol{T} \end{bmatrix} \tag{14}$$

with $\eta = \sqrt{\lambda_1^2 + \lambda_2^2}$.

Thus, based on the variables we have introduced and in the Fourier-transformed domain, the governing equation (3) in the absence of the extended body source becomes

$$\begin{aligned} &C_{3IK3}\tilde{u}_{K,33} - \mathrm{i}(C_{\alpha IK3} + C_{3IK\alpha})\lambda_\alpha \tilde{u}_{K,3} R/a_\alpha \\ &\quad - C_{\alpha IK\beta}\lambda_\alpha \lambda_\beta \tilde{u}_K R^2/(a_\alpha a_\beta) = 0, \end{aligned} \tag{15}$$

where the repeated Greek indices α and β take the summation from 1 to 2.

We now introduce the polar coordinates (η, θ) which are related to the variables (λ_1, λ_2) as

$$\begin{bmatrix}\lambda_1\\ \lambda_2\\ 0\end{bmatrix} = \eta \boldsymbol{m},$$
$$\boldsymbol{m} = \begin{bmatrix}m_1\\ m_2\\ 0\end{bmatrix} = \begin{bmatrix}\cos\theta\\ \sin\theta\\ 0\end{bmatrix}, \qquad \boldsymbol{n} = \begin{bmatrix}0\\ 0\\ 1\end{bmatrix}, \tag{16}$$

where $\boldsymbol{m}$ and $\boldsymbol{n}$ are the two unit vectors which are normal to each other. This polar coordinate system is required later in the Stroh formalism.

The general solution of equation (15) can be assumed as

$$\tilde{\boldsymbol{u}}(\lambda_1, \lambda_2, x_3) = \boldsymbol{a}\mathrm{e}^{-\mathrm{i}p\eta x_3}. \tag{17}$$

Substituting equation (17) into equation (15) gives us the following eigenequation system:

$$[\boldsymbol{Q} + p(\boldsymbol{R} + \boldsymbol{R}^t) + p^2\boldsymbol{T}]\boldsymbol{a} = \boldsymbol{0}, \tag{18}$$

with

$$Q_{IK} = C_{\alpha IK\beta}m_\alpha m_\beta R^2/(a_\alpha a_\beta),$$
$$R_{IK} = C_{\alpha IK3}m_\alpha R/a_\alpha, \qquad T_{IK} = C_{3IK3}. \tag{19}$$

Without loss of generality, we assume that the first five eigenpairs of the eigenvalues p_J of equation (18) satisfy condition $\mathrm{Im}(p_J) > 0$ and that the associated eigenvectors are $\boldsymbol{a}_J$. The remaining five eigenpairs are then obtained simply by $p_{J+5} = \bar{p}_J$, $\boldsymbol{a}_{J+5} = \bar{\boldsymbol{a}}_J$ (J = 1–5). Hence the general solution of the extended displacement in the Fourier-transformed domain is

$$\tilde{\boldsymbol{u}}(\lambda_1, \lambda_2, x_3) = \mathrm{i}\eta^{-1}\bar{\boldsymbol{A}}\langle \mathrm{e}^{-\mathrm{i}\bar{p}_*\eta x_3}\rangle\bar{\boldsymbol{q}} + \mathrm{i}\eta^{-1}\boldsymbol{A}\langle \mathrm{e}^{-\mathrm{i}p_*\eta x_3}\rangle\boldsymbol{q}', \tag{20}$$

where the overbar denotes the complex conjugate, $\bar{\boldsymbol{q}}$ and $\boldsymbol{q}'$ are two unknown complex vectors, and the matrices $\langle \mathrm{e}^{-\mathrm{i}p_*\eta x_3}\rangle$ and $\boldsymbol{A}$ are defined as

$$\langle \mathrm{e}^{-\mathrm{i}p_*\eta x_3}\rangle = \mathrm{diag}[\mathrm{e}^{-\mathrm{i}p_1\eta x_3}, \mathrm{e}^{-\mathrm{i}p_2\eta x_3}, \mathrm{e}^{-\mathrm{i}p_3\eta x_3},$$
$$\mathrm{e}^{-\mathrm{i}p_4\eta x_3}, \mathrm{e}^{-\mathrm{i}p_5\eta x_3}], \qquad \boldsymbol{A} = [\boldsymbol{a}_1, \boldsymbol{a}_2, \boldsymbol{a}_3, \boldsymbol{a}_4, \boldsymbol{a}_5]. \tag{21}$$

In order to use the boundary conditions in equations (4)–(7) to determine the unknown vectors $\bar{\boldsymbol{q}}$ and $\boldsymbol{q}'$, we also need the expression for the extended stresses. The extended stresses on the x_3 = constant plane are divided into two parts: the extended traction vector

$$\boldsymbol{t} = (\sigma_{31}, \sigma_{32}, \sigma_{33}, \sigma_{34}, \sigma_{35})^{\mathrm{T}}$$
$$= (\sigma_{31}, \sigma_{32}, \sigma_{33}, D_3, B_3)^{\mathrm{T}} \tag{22}$$

and the extended in-plane stress vector

$$\boldsymbol{s} = (\sigma_{11}, \sigma_{12}, \sigma_{22}, \sigma_{14}, \sigma_{24}, \sigma_{15}, \sigma_{25})^{\mathrm{T}}$$
$$\equiv (\sigma_{11}, \sigma_{12}, \sigma_{22}, D_1, D_2, B_1, B_2)^{\mathrm{T}}. \tag{23}$$

Making use of the constitutive relation equation (2) and the general solution of the extended displacement equation (20), the extended stresses in the Fourier-transformed domain can be written as

$$\tilde{\boldsymbol{t}}(\lambda_1, \lambda_2, x_3) = \bar{\boldsymbol{B}}\langle \mathrm{e}^{-\mathrm{i}\bar{p}_*\eta x_3}\rangle\bar{\boldsymbol{q}} + \boldsymbol{B}\langle \mathrm{e}^{-\mathrm{i}p_*\eta x_3}\rangle\boldsymbol{q}',$$
$$\tilde{\boldsymbol{s}}(\lambda_1, \lambda_2, x_3) = \bar{\boldsymbol{C}}\langle \mathrm{e}^{-\mathrm{i}\bar{p}_*\eta x_3}\rangle\bar{\boldsymbol{q}} + \boldsymbol{C}\langle \mathrm{e}^{-\mathrm{i}p_*\eta x_3}\rangle\boldsymbol{q}', \tag{24}$$

where $\boldsymbol{B} \equiv [\boldsymbol{b}_1, \boldsymbol{b}_2, \boldsymbol{b}_3, \boldsymbol{b}_4, \boldsymbol{b}_5]$ and $\boldsymbol{C}$ (7×5) are determined by the eigenvalues and related eigenvectors, i.e.,

$$\boldsymbol{B} = \boldsymbol{R}^t\boldsymbol{A} + \boldsymbol{TAP}; \qquad \boldsymbol{C} = \boldsymbol{H}_\alpha \boldsymbol{ARm}_\alpha/a_\alpha + \boldsymbol{JAP} \tag{25}$$

with

$$\boldsymbol{P} = \mathrm{diag}[p_1, p_2, p_3, p_4, p_5]$$

$$\boldsymbol{H}_\alpha \equiv \begin{bmatrix} C_{111\alpha} & C_{112\alpha} & C_{113\alpha} & C_{114\alpha} & C_{115\alpha}\\ C_{121\alpha} & C_{122\alpha} & C_{123\alpha} & C_{124\alpha} & C_{125\alpha}\\ C_{221\alpha} & C_{222\alpha} & C_{223\alpha} & C_{224\alpha} & C_{225\alpha}\\ C_{141\alpha} & C_{142\alpha} & C_{143\alpha} & C_{144\alpha} & C_{145\alpha}\\ C_{241\alpha} & C_{242\alpha} & C_{243\alpha} & C_{244\alpha} & C_{245\alpha}\\ C_{151\alpha} & C_{152\alpha} & C_{153\alpha} & C_{154\alpha} & C_{155\alpha}\\ C_{251\alpha} & C_{252\alpha} & C_{253\alpha} & C_{254\alpha} & C_{255\alpha} \end{bmatrix},$$

$$\boldsymbol{J} \equiv \begin{bmatrix} C_{1113} & C_{1123} & C_{1133} & C_{1143} & C_{1153}\\ C_{1213} & C_{1223} & C_{1233} & C_{1243} & C_{1253}\\ C_{2213} & C_{2223} & C_{2233} & C_{2243} & C_{2253}\\ C_{1413} & C_{1423} & C_{1433} & C_{1443} & C_{1453}\\ C_{2413} & C_{2423} & C_{2433} & C_{2443} & C_{2453}\\ C_{1513} & C_{1523} & C_{1533} & C_{1543} & C_{1553}\\ C_{2513} & C_{2523} & C_{2533} & C_{2543} & C_{2553} \end{bmatrix},$$

where the repeated index α takes the summation from 1 to 2. It is obvious that when the elliptical region is reduced to a circular one, our formulations are reduced to those in Zhao *et al* (2013).

It should be also noted that the eigenmatrix $\boldsymbol{A}$ defined in equation (21) is calculated from equation (18), and the matrices $\boldsymbol{B}$ and $\boldsymbol{C}$ are from equation (25). These matrices, the vectors $\bar{\boldsymbol{q}}$ and $\boldsymbol{q}'$, as well as the eigenvalues p_J in solutions (20) and (24) are all functions of the circumferential polar coordinate θ, as defined in equation (16).

Since the elliptical loading region is scaled into a circular one in this section, the general solutions in the three subdomains in the Fourier and physical domains can be easily derived as in Zhao *et al* (2013). In what follows, we only present the main results as the details can be found in Zhao *et al* (2013).

3.2. The general Fourier domain solution in the three subdomains

In the Fourier-transformed domain, the continuity conditions (4) on the interface $x_3 = 0$ becomes

$$\tilde{\boldsymbol{u}}|_{x_3=0^+} - \tilde{\boldsymbol{u}}|_{x_3=0^-} = \boldsymbol{0}; \qquad \tilde{\boldsymbol{t}}|_{x_3=0^+} - \tilde{\boldsymbol{t}}|_{x_3=0^-} = \boldsymbol{0}. \tag{26}$$

On the loading level $x_3 = h$, the discontinuity conditions (5) and (6) in the Fourier domain are

$$\tilde{\boldsymbol{u}}|_{x_3=h^+} - \tilde{\boldsymbol{u}}|_{x_3=h^-} = \tilde{\boldsymbol{d}} \tag{27}$$

$$\tilde{\boldsymbol{t}}|_{x_3=h^+} - \tilde{\boldsymbol{t}}|_{x_3=h^-} = \tilde{\boldsymbol{T}}, \tag{28}$$

where $\tilde{\boldsymbol{d}}$ and $\tilde{\boldsymbol{T}}$ are, respectively, the Fourier transformation of the given uniform dislocation and traction over the elliptical region as derived in equation (14).

In addition, condition (7) at infinity in the Fourier-transformed domain becomes

$$\lim_{|\boldsymbol{x}|\to\infty} \tilde{u}_J = 0, \qquad \lim_{|\boldsymbol{x}|\to\infty} \tilde{\sigma}_{iJ} = 0. \tag{29}$$

As in Pan and Yuan (2000), we now assume that the solution in the upper half-space contains two parts—the full-space solution and a complementary part, whilst the solution in the lower half-space contains only the complementary part. In other words, the solutions in the three Fourier-transformed subdomains can be expressed as follows.

For $x_3 > h$ (in Material 1):

$$\begin{aligned}
\tilde{\boldsymbol{u}}^{(1)}(\lambda_1,\lambda_2,x_3) &= \pm \mathrm{i}\eta^{-1}\bar{\boldsymbol{A}}^{(1)}\langle \mathrm{e}^{-\mathrm{i}\bar{p}_*^{(1)}\eta(x_3-h)}\rangle \bar{\boldsymbol{q}}^{\infty} \\
&\quad - \mathrm{i}\eta^{-1}\bar{\boldsymbol{A}}^{(1)}\langle \mathrm{e}^{-\mathrm{i}\bar{p}_*^{(1)}\eta x_3}\rangle \bar{\boldsymbol{q}}^{(1)} \\
\tilde{\boldsymbol{t}}^{(1)}(\lambda_1,\lambda_2,x_3) &= \pm \bar{\boldsymbol{B}}^{(1)}\langle \mathrm{e}^{-\mathrm{i}\bar{p}_*^{(1)}\eta(x_3-h)}\rangle \bar{\boldsymbol{q}}^{\infty} \\
&\quad - \bar{\boldsymbol{B}}^{(1)}\langle \mathrm{e}^{-\mathrm{i}\bar{p}_*^{(1)}\eta x_3}\rangle \bar{\boldsymbol{q}}^{(1)} \\
\tilde{\boldsymbol{s}}^{(1)}(\lambda_1,\lambda_2,x_3) &= \pm \bar{\boldsymbol{C}}^{(1)}\langle \mathrm{e}^{-\mathrm{i}\bar{p}_*^{(1)}\eta(x_3-h)}\rangle \bar{\boldsymbol{q}}^{\infty} \\
&\quad - \bar{\boldsymbol{C}}^{(1)}\langle \mathrm{e}^{-\mathrm{i}\bar{p}_*^{(1)}\eta x_3}\rangle \bar{\boldsymbol{q}}^{(1)}.
\end{aligned} \tag{30}$$

For $0 \le x_3 < h$ (in Material 1):

$$\begin{aligned}
\tilde{\boldsymbol{u}}^{(1)}(\lambda_1,\lambda_2,x_3) &= \mathrm{i}\eta^{-1}\boldsymbol{A}^{(1)}\langle \mathrm{e}^{-\mathrm{i}p_*^{(1)}\eta(x_3-h)}\rangle \boldsymbol{q}^{\infty} \\
&\quad - \mathrm{i}\eta^{-1}\bar{\boldsymbol{A}}^{(1)}\langle \mathrm{e}^{-\mathrm{i}\bar{p}_*^{(1)}\eta x_3}\rangle \bar{\boldsymbol{q}}^{(1)} \\
\tilde{\boldsymbol{t}}^{(1)}(\lambda_1,\lambda_2,x_3) &= \boldsymbol{B}^{(1)}\langle \mathrm{e}^{-\mathrm{i}p_*^{(1)}\eta(x_3-h)}\rangle \boldsymbol{q}^{\infty} \\
&\quad - \bar{\boldsymbol{B}}^{(1)}\langle \mathrm{e}^{-\mathrm{i}\bar{p}_*^{(1)}\eta x_3}\rangle \bar{\boldsymbol{q}}^{(1)} \\
\tilde{\boldsymbol{s}}^{(1)}(\lambda_1,\lambda_2,x_3) &= \boldsymbol{C}^{(1)}\langle \mathrm{e}^{-\mathrm{i}p_*^{(1)}\eta(x_3-h)}\rangle \boldsymbol{q}^{\infty} \\
&\quad - \bar{\boldsymbol{C}}^{(1)}\langle \mathrm{e}^{-\mathrm{i}\bar{p}_*^{(1)}\eta x_3}\rangle \bar{\boldsymbol{q}}^{(1)}.
\end{aligned} \tag{31}$$

For $x_3 < 0$ (in Material 2):

$$\begin{aligned}
\tilde{\boldsymbol{u}}^{(2)}(\lambda_1,\lambda_2,x_3) &= \mathrm{i}\eta^{-1}\boldsymbol{A}^{(2)}\langle \mathrm{e}^{-\mathrm{i}p_*^{(2)}\eta x_3}\rangle \boldsymbol{q}^{(2)} \\
\tilde{\boldsymbol{t}}^{(2)}(\lambda_1,\lambda_2,x_3) &= \boldsymbol{B}^{(2)}\langle \mathrm{e}^{-\mathrm{i}p_*^{(2)}\eta x_3}\rangle \boldsymbol{q}^{(2)} \\
\tilde{\boldsymbol{s}}^{(2)}(\lambda_1,\lambda_2,x_3) &= \boldsymbol{C}^{(2)}\langle \mathrm{e}^{-\mathrm{i}p_*^{(2)}\eta x_3}\rangle \boldsymbol{q}^{(2)}
\end{aligned} \tag{32}$$

where the superscripts '(1)' and '(2)' denote, respectively, the quantities in Materials 1 and 2, and $\bar{\boldsymbol{q}}^{(1)}$, $\boldsymbol{q}^{(2)}$ and $\boldsymbol{q}^{\infty}$ are the three unknown vectors to be determined by conditions (26)–(29). It should be noted that the positive '+' and negative '−' signs in equation (30) correspond to the dislocation and traction cases, respectively.

3.3. Determination of unknown vectors in the solutions

First, the complex vector $\boldsymbol{q}^{\infty}$ can be determined by the discontinuity condition in equations (27) and (28) at $x_3 = h$. By means of the orthogonal normalization identity (Ting 1996) we can verify that the discontinuity condition in equations (27) and (28) are satisfied if the unknown vector $\boldsymbol{q}^{\infty}$ in equations (30) and (31) takes the following expression:

$$\boldsymbol{q}^{\infty} = \begin{cases} -\mathrm{i}\eta(\boldsymbol{B}^{(1)})^{\mathrm{T}}\tilde{\boldsymbol{d}} & \text{(for dislocation)} \\ (\boldsymbol{A}^{(1)})^{\mathrm{T}}\tilde{\boldsymbol{T}} & \text{(for traction).} \end{cases} \tag{33}$$

Then, substituting the solution equations (31) and (32) into continuity conditions (26) on the interface $x_3 = 0$ yields

$$\begin{aligned}
\boldsymbol{A}^{(2)}\boldsymbol{q}^{(2)} + \bar{\boldsymbol{A}}^{(1)}\bar{\boldsymbol{q}}^{(1)} &= \boldsymbol{A}^{(1)}\langle \mathrm{e}^{\mathrm{i}p_*^{(1)}\eta h}\rangle \boldsymbol{q}^{\infty} \\
\boldsymbol{B}^{(2)}\boldsymbol{q}^{(2)} + \bar{\boldsymbol{B}}^{(1)}\bar{\boldsymbol{q}}^{(1)} &= \boldsymbol{B}^{(1)}\langle \mathrm{e}^{\mathrm{i}p_*^{(1)}\eta h}\rangle \boldsymbol{q}^{\infty}.
\end{aligned} \tag{34}$$

To solve the unknown vectors $\bar{\boldsymbol{q}}^{(1)}$ and $\boldsymbol{q}^{(2)}$ from equation (34), we introduce the matrices

$$\boldsymbol{M}^{(\alpha)} = -\mathrm{i}\boldsymbol{B}^{(\alpha)}(\boldsymbol{A}^{(\alpha)})^{-1} \qquad (\alpha = 1, 2). \tag{35}$$

Substituting $\boldsymbol{B}^{(\alpha)} = \mathrm{i}\boldsymbol{M}^{(\alpha)}\boldsymbol{A}^{(\alpha)}$ $(\alpha = 1, 2)$ into equation (34) and solving for the unknown vectors, we obtain

$$\begin{aligned}
\bar{\boldsymbol{q}}^{(1)} &= \boldsymbol{G}_1\langle \mathrm{e}^{\mathrm{i}p_*^{(1)}\eta h}\rangle \boldsymbol{q}^{\infty} \\
\boldsymbol{q}^{(2)} &= \boldsymbol{G}_2\langle \mathrm{e}^{\mathrm{i}p_*^{(1)}\eta h}\rangle \boldsymbol{q}^{\infty},
\end{aligned} \tag{36}$$

where the matrices $\boldsymbol{G}_1$ and $\boldsymbol{G}_2$ are defined by

$$\begin{aligned}
\boldsymbol{G}_1 &= -(\bar{\boldsymbol{A}}^{(1)})^{-1}(\bar{\boldsymbol{M}}^{(1)} + \boldsymbol{M}^{(2)})^{-1}(\boldsymbol{M}^{(1)} - \boldsymbol{M}^{(2)})\boldsymbol{A}^{(1)} \\
\boldsymbol{G}_2 &= (\boldsymbol{A}^{(2)})^{-1}(\bar{\boldsymbol{M}}^{(1)} + \boldsymbol{M}^{(2)})^{-1}(\boldsymbol{M}^{(1)} + \bar{\boldsymbol{M}}^{(1)})\boldsymbol{A}^{(1)}.
\end{aligned} \tag{37}$$

3.4. General solution in the physical domain

By introducing

$$\begin{aligned}
y_1 &= r\cos\varphi \\
y_2 &= r\sin\varphi
\end{aligned} \tag{38}$$

the inverse Fourier transformation in terms of polar coordinates becomes

$$F(y_1, y_2, x_3) = \frac{1}{4\pi^2}\int_0^{2\pi} \mathrm{d}\theta \int_0^{\infty} \tilde{F}(\lambda_1,\lambda_2,x_3)\mathrm{e}^{-\mathrm{i}r\eta\cos(\varphi-\theta)}\eta\,\mathrm{d}\eta. \tag{39}$$

Applying equation (39) to equations (30)–(32), we obtain the extended displacements and stresses in the three physical subdomains as follows.

For $x_3 > h$ (in Material 1):

$$\begin{bmatrix} \boldsymbol{u}^{(1)}(r,\varphi,x_3) \\ \boldsymbol{t}^{(1)}(r,\varphi,x_3) \\ \boldsymbol{s}^{(1)}(r,\varphi,x_3) \end{bmatrix} = \frac{1}{4\pi^2}\int_0^{2\pi}\int_0^{\infty} \left(\pm \begin{bmatrix} \mathrm{i}\eta^{-1}\bar{\boldsymbol{A}}^{(1)} \\ \bar{\boldsymbol{B}}^{(1)} \\ \bar{\boldsymbol{C}}^{(1)} \end{bmatrix} \boldsymbol{K}_+^{\infty}\bar{\boldsymbol{q}}^{\infty} - \begin{bmatrix} \mathrm{i}\eta^{-1}\bar{\boldsymbol{A}}^{(1)} \\ \bar{\boldsymbol{B}}^{(1)} \\ \bar{\boldsymbol{C}}^{(1)} \end{bmatrix} \boldsymbol{K}_1\boldsymbol{q}^{\infty} \right) \eta\,\mathrm{d}\eta\,\mathrm{d}\theta. \tag{40}$$

For $0 \le x_3 < h$ (in Material 1):

$$\begin{bmatrix} \boldsymbol{u}^{(1)}(r,\varphi,x_3) \\ \boldsymbol{t}^{(1)}(r,\varphi,x_3) \\ \boldsymbol{s}^{(1)}(r,\varphi,x_3) \end{bmatrix} = \frac{1}{4\pi^2}\int_0^{2\pi}\int_0^{\infty} \left(\begin{bmatrix} \mathrm{i}\eta^{-1}\boldsymbol{A}^{(1)} \\ \boldsymbol{B}^{(1)} \\ \boldsymbol{C}^{(1)} \end{bmatrix} \boldsymbol{K}_-^{\infty}\boldsymbol{q}^{\infty} - \begin{bmatrix} \mathrm{i}\eta^{-1}\bar{\boldsymbol{A}}^{(1)} \\ \bar{\boldsymbol{B}}^{(1)} \\ \bar{\boldsymbol{C}}^{(1)} \end{bmatrix} \boldsymbol{K}_1\boldsymbol{q}^{\infty} \right) \eta\,\mathrm{d}\eta\,\mathrm{d}\theta. \tag{41}$$

For $x_3 < 0$ (in Material 2):

$$\begin{bmatrix} \boldsymbol{u}^{(2)}(r,\varphi,x_3) \\ \boldsymbol{t}^{(2)}(r,\varphi,x_3) \\ \boldsymbol{s}^{(2)}(r,\varphi,x_3) \end{bmatrix} = \frac{1}{4\pi^2}\int_0^{2\pi}\int_0^{\infty}\begin{bmatrix} \mathrm{i}\eta^{-1}\boldsymbol{A}^{(2)} \\ \boldsymbol{B}^{(2)} \\ \boldsymbol{C}^{(2)} \end{bmatrix}\boldsymbol{K}_2\boldsymbol{q}^{\infty}\eta\,\mathrm{d}\eta\,\mathrm{d}\theta, \tag{42}$$

where the signs '+' and '−' in solution (40) again correspond, respectively, to the dislocation and traction case, and the involved matrices are defined as

$$\begin{aligned} (\boldsymbol{K}_+^{\infty})_{IJ} &= \mathrm{e}^{-\mathrm{i}\eta[r\cos(\varphi-\theta)+\bar{p}_I^{(1)}(x_3-h)]}\boldsymbol{\delta}_{IJ}, \\ (\boldsymbol{K}_-^{\infty})_{IJ} &= \mathrm{e}^{-\mathrm{i}\eta[r\cos(\varphi-\theta)+p_I^{(1)}(x_3-h)]}\boldsymbol{\delta}_{IJ}, \\ (\boldsymbol{K}_1)_{IJ} &= \mathrm{e}^{-\mathrm{i}\eta[r\cos(\varphi-\theta)+\bar{p}_I^{(1)}x_3-p_J^{(1)}h]}(\boldsymbol{G}_1)_{IJ}, \\ (\boldsymbol{K}_2)_{IJ} &= \mathrm{e}^{-\mathrm{i}\eta[r\cos(\varphi-\theta)+p_I^{(2)}x_3-p_J^{(1)}h]}(\boldsymbol{G}_2)_{IJ}, \end{aligned} \tag{43}$$

where the eigenvalues p_I are calculated from the eigenequation (18).

Up to now, in the three physical domains, we have obtained the general solutions (40)–(42) which are expressed by two-dimensional integrals in the transformed space (η,θ). In those solutions, for each material domain ($\alpha = 1, 2$), the eigenvalues $p_I^{(\alpha)}$ ($I = 1, 2, \ldots, 5$) and eigenmatrix $\boldsymbol{A}^{(\alpha)}$ can be solved from the eigenequation (18), the matrices $\boldsymbol{B}^{(\alpha)}$ and $\boldsymbol{C}^{(\alpha)}$ are from relation (25), and the matrices $\boldsymbol{G}_\alpha$ can be calculated from equation (37). They are all functions of the variable θ only. The vector $\boldsymbol{q}^{\infty}$ is given by equation (33), and thus, in general, is associated with both θ and η. However, for the uniform traction and dislocation loading cases, the involved infinite integral with respect to η can be carried out. This is discussed below.

4. Solutions for uniform dislocation and traction cases

To carry out the infinite integral with respect to η in equations (40)–(42), the following infinite integral formulas (Watson 1966) will be used:

$$\int_0^{\infty}\mathrm{e}^{-at}J_1(bt)\begin{bmatrix} t^{-1} \\ 1 \\ t \end{bmatrix}\mathrm{d}t = \begin{bmatrix} \frac{1}{b}\left(\sqrt{a^2+b^2}-a\right) \\ \frac{1}{b}\left(1-\frac{a}{\sqrt{a^2+b^2}}\right) \\ \frac{b}{(a^2+b^2)^{3/2}} \end{bmatrix}, \tag{44}$$

under the condition $\mathrm{Re}(a) > 0$. We present the analytical solutions below for both traction and dislocation loading cases.

4.1. Solutions for uniform extended dislocation case

Substituting the first expression in equation (14) into equation (33), and then equations (40)–(42), and making use of equation (44), we obtain the simple analytical solutions in the three subdomains as follows.

For $x_3 > h$ (in Material 1):

$$\begin{bmatrix} \boldsymbol{u}^{(1)}(r,\varphi,x_3) \\ \boldsymbol{t}^{(1)}(r,\varphi,x_3) \\ \boldsymbol{s}^{(1)}(r,\varphi,x_3) \end{bmatrix} = \frac{1}{2\pi}\int_0^{2\pi}\left(-\begin{bmatrix} \bar{\boldsymbol{A}}^{(1)}\boldsymbol{G}_u^{h+} \\ \bar{\boldsymbol{B}}^{(1)}\boldsymbol{G}_\sigma^{h+} \\ \bar{\boldsymbol{C}}^{(1)}\boldsymbol{G}_\sigma^{h+} \end{bmatrix}(\bar{\boldsymbol{B}}^{(1)})^{\mathrm{T}} - \begin{bmatrix} \bar{\boldsymbol{A}}^{(1)}\boldsymbol{G}_u^{(1)} \\ \bar{\boldsymbol{B}}^{(1)}\boldsymbol{G}_\sigma^{(1)} \\ \bar{\boldsymbol{C}}^{(1)}\boldsymbol{G}_\sigma^{(1)} \end{bmatrix}(\boldsymbol{B}^{(1)})^{\mathrm{T}}\right)\mathrm{d}\theta\,\boldsymbol{d}. \tag{45}$$

For $0 \le x_3 < h$ (in Material 1):

$$\begin{bmatrix} \boldsymbol{u}^{(1)}(r,\varphi,x_3) \\ \boldsymbol{t}^{(1)}(r,\varphi,x_3) \\ \boldsymbol{s}^{(1)}(r,\varphi,x_3) \end{bmatrix} = \frac{1}{2\pi}\int_0^{2\pi}\begin{bmatrix} \boldsymbol{A}^{(1)}\boldsymbol{G}_u^{h-}-\bar{\boldsymbol{A}}^{(1)}\boldsymbol{G}_u^{(1)} \\ \boldsymbol{B}^{(1)}\boldsymbol{G}_\sigma^{h-}-\bar{\boldsymbol{B}}^{(1)}\boldsymbol{G}_\sigma^{(1)} \\ \boldsymbol{C}^{(1)}\boldsymbol{G}_\sigma^{h-}-\bar{\boldsymbol{C}}^{(1)}\boldsymbol{G}_\sigma^{(1)} \end{bmatrix}(\boldsymbol{B}^{(1)})^{\mathrm{T}}\,\mathrm{d}\theta\,\boldsymbol{d}. \tag{46}$$

For $x_3 < 0$ (in Material 2):

$$\begin{bmatrix} \boldsymbol{u}^{(2)}(r,\varphi,x_3) \\ \boldsymbol{t}^{(2)}(r,\varphi,x_3) \\ \boldsymbol{s}^{(2)}(r,\varphi,x_3) \end{bmatrix} = \frac{1}{2\pi}\int_0^{2\pi}\begin{bmatrix} \boldsymbol{A}^{(2)}\boldsymbol{G}_u^{(2)} \\ \boldsymbol{B}^{(2)}\boldsymbol{G}_\sigma^{(2)} \\ \boldsymbol{C}^{(2)}\boldsymbol{G}_\sigma^{(2)} \end{bmatrix}(\boldsymbol{B}^{(1)})^{\mathrm{T}}\,\mathrm{d}\theta\,\boldsymbol{d}, \tag{47}$$

where

$$\begin{aligned} &(\boldsymbol{G}_u^{h\pm})_{IJ} \\ &\quad = \left(1-\frac{\mathrm{i}[r\cos(\varphi-\theta)+p_I^{\pm}(x_3-h)]}{\sqrt{R^2-[r\cos(\varphi-\theta)+p_I^{\pm}(x_3-h)]^2}}\right)\boldsymbol{\delta}_{IJ}, \\ &(\boldsymbol{G}_u^{(\alpha)})_{IJ} \\ &\quad = \left(1-\frac{\mathrm{i}[r\cos(\varphi-\theta)+\hat{p}_I^{(\alpha)}x_3-p_J^{(1)}h]}{\sqrt{R^2-[r\cos(\varphi-\theta)+\hat{p}_I^{(\alpha)}x_3-p_J^{(1)}h]^2}}\right)(\boldsymbol{G}_\alpha)_{IJ}, \\ &(\boldsymbol{G}_\sigma^{h\pm})_{IJ} \\ &\quad = \frac{-\mathrm{i}R^2}{(R^2-[r\cos(\varphi-\theta)+p_I^{\pm}(x_3-h)]^2)^{3/2}}\boldsymbol{\delta}_{IJ}, \\ &(\boldsymbol{G}_\sigma^{(\alpha)})_{IJ} \\ &\quad = \frac{-\mathrm{i}R^2}{(R^2-[r\cos(\varphi-\theta)+\hat{p}_I^{(\alpha)}x_3-p_J^{(1)}h]^2)^{3/2}}(\boldsymbol{G}_\alpha)_{IJ}. \end{aligned} \tag{48}$$

In equation (48) and below we introduce $\hat{p}_I^{(1)} = \bar{p}_I^{(1)}$, $\hat{p}_I^{(2)} = p_I^{(2)}$, $p_I^{+} = \bar{p}_I^{(1)}$, $p_I^{-} = p_I^{(1)}$, $\alpha = 1, 2$.

4.2. Solutions for extended uniform traction case

Similarly, substituting the second expression in equation (14) into equation (33) and then equations (40)–(42), and making use of equation (44), we have the following analytical solutions in the three physical domains.

For $x_3 > h$ (in Material 1):

$$\begin{bmatrix} \boldsymbol{u}^{(1)}(r,\varphi,x_3) \\ \boldsymbol{t}^{(1)}(r,\varphi,x_3) \\ \boldsymbol{s}^{(1)}(r,\varphi,x_3) \end{bmatrix} = \frac{1}{2\pi}\int_0^{2\pi}\left(-\begin{bmatrix} \bar{\boldsymbol{A}}^{(1)}\boldsymbol{G}_u^{h+} \\ \bar{\boldsymbol{B}}^{(1)}\boldsymbol{G}_\sigma^{h+} \\ \bar{\boldsymbol{C}}^{(1)}\boldsymbol{G}_\sigma^{h+} \end{bmatrix}(\bar{\boldsymbol{A}}^{(1)})^{\mathrm{T}} - \begin{bmatrix} \bar{\boldsymbol{A}}^{(1)}\boldsymbol{G}_u^{(1)} \\ \bar{\boldsymbol{B}}^{(1)}\boldsymbol{G}_\sigma^{(1)} \\ \bar{\boldsymbol{C}}^{(1)}\boldsymbol{G}_\sigma^{(1)} \end{bmatrix}(\boldsymbol{A}^{(1)})^{\mathrm{T}}\right)\mathrm{d}\theta\,\boldsymbol{T}. \quad (49)$$

For $0 \le x_3 < h$ (in Material 1):

$$\begin{bmatrix} \boldsymbol{u}^{(1)}(r,\varphi,x_3) \\ \boldsymbol{t}^{(1)}(r,\varphi,x_3) \\ \boldsymbol{s}^{(1)}(r,\varphi,x_3) \end{bmatrix} = \frac{1}{2\pi}\int_0^{2\pi}\begin{bmatrix} \boldsymbol{A}^{(1)}\boldsymbol{G}_u^{h-} - \bar{\boldsymbol{A}}^{(1)}\boldsymbol{G}_u^{(1)} \\ \boldsymbol{B}^{(1)}\boldsymbol{G}_\sigma^{h-} - \bar{\boldsymbol{B}}^{(1)}\boldsymbol{G}_\sigma^{(1)} \\ \boldsymbol{C}^{(1)}\boldsymbol{G}_\sigma^{h-} - \bar{\boldsymbol{C}}^{(1)}\boldsymbol{G}_\sigma^{(1)} \end{bmatrix}(\boldsymbol{A}^{(1)})^{\mathrm{T}}\,\mathrm{d}\theta\,\boldsymbol{T}. \quad (50)$$

For $x_3 < 0$ (in Material 2):

$$\begin{bmatrix} \boldsymbol{u}^{(2)}(r,\varphi,x_3) \\ \boldsymbol{t}^{(2)}(r,\varphi,x_3) \\ \boldsymbol{s}^{(2)}(r,\varphi,x_3) \end{bmatrix} = \frac{1}{2\pi}\int_0^{2\pi}\begin{bmatrix} \boldsymbol{A}^{(2)}\boldsymbol{G}_u^{(2)} \\ \boldsymbol{B}^{(2)}\boldsymbol{G}_\sigma^{(2)} \\ \boldsymbol{C}^{(2)}\boldsymbol{G}_\sigma^{(2)} \end{bmatrix}(\boldsymbol{A}^{(1)})^{\mathrm{T}}\,\mathrm{d}\theta\,\boldsymbol{T}, \quad (51)$$

where

$$\begin{aligned}
(\boldsymbol{G}_u^{h\pm})_{IJ} &= -\Big([r\cos(\varphi-\theta) + p_I^{\pm}(x_3-h)] \\
&\quad + \mathrm{i}\sqrt{R^2 - [r\cos(\varphi-\theta) + p_I^{\pm}(x_3-h)]^2}\Big)\boldsymbol{\delta}_{IJ} \\
(\boldsymbol{G}_u^{(\alpha)})_{IJ} &= \Big([r\cos(\varphi-\theta) + \hat{p}_I^{(\alpha)}x_3 - p_J^{(1)}h] \\
&\quad + \mathrm{i}\sqrt{R^2 - [r\cos(\varphi-\theta) + \hat{p}_I^{(\alpha)}x_3 - p_J^{(1)}h]^2}\Big)(\boldsymbol{G}_\alpha)_{IJ} \\
(\boldsymbol{G}_\sigma^{h\pm})_{IJ} &= \left(1 - \frac{\mathrm{i}[r\cos(\varphi-\theta) + p_I^{\pm}(x_3-h)]}{\sqrt{R^2 - [r\cos(\varphi-\theta) + p_I^{\pm}(x_3-h)]^2}}\right)\boldsymbol{\delta}_{IJ}, \\
(\boldsymbol{G}_\sigma^{(\alpha)})_{IJ} &= \left(1 - \frac{\mathrm{i}[r\cos(\varphi-\theta) + \hat{p}_I^{(\alpha)}x_3 - p_J^{(1)}h]}{\sqrt{R^2 - [r\cos(\varphi-\theta) + \hat{p}_I^{(\alpha)}x_3 - p_J^{(1)}h]^2}}\right)(\boldsymbol{G}_\alpha)_{IJ}.
\end{aligned} \quad (52)$$

Finally, for fixed x_3, after we find the solution in the (y_1, y_2)-plane (in terms of r and φ), we need to transform the solution back to the real physical plane (x_1, x_2) by the following simple transform:

$$x_1 = r\cos\varphi\frac{a_1}{R}; \qquad x_2 = r\sin\varphi\frac{a_2}{R}. \quad (53)$$

5. Numerical examples and discussion

Before applying our analytical solutions to numerical examples, we first validated our solutions. For instance, for a reduced purely elastic isotropic half-space under a uniform vertical traction over an elliptical area with its minor and major radii being $a_1 = 0.8$ (m), $a_2 = 1.0$ (m) ($a_1/a_2 = 0.8$) on the surface of the half-space, the vertical displacement and three principal stresses along the z-axis from the present formulation are exactly the same as those in Deresiewicz (1960). We have also reduced our solutions to the special circular loading case and found that the reduced results are the same as those in Zhao *et al* (2013).

In the numerical examples, two transversely isotropic materials, i.e., the pseudo-BaTiO$_3$ (Pan 2002) and the MEE composite made of 50% BaTiO$_3$ and 50% CoFe$_2$O$_4$ (Xue *et al* 2011), are chosen as the upper and lower half-space materials, respectively.

5.1. Field response on the interface

In this section, the material coordinate system of both the upper and lower half-spaces is selected such that the axis of material symmetry is along the global x_3-axis. The field response on the interface under uniform horizontal dislocation and uniform horizontal traction is analyzed by considering the effect of different elliptical semi-axes ratios. Since for the loading over an elliptical region with semi-axes a_1 and a_2, the area of the ellipse is

$$S_{\text{area}} = \pi a_1 a_2 \equiv \pi R^2, \quad (54)$$

we select the length scale $R \equiv \sqrt{a_1 a_2}$ to normalize our numerical results. Three different pairs of semi-axes a_1 and a_2 are considered: (1) $a_1/R = 0.5$, $a_2/R = 2.0$; (2) $a_1/R = 1.0$, $a_2/R = 1.0$; (3) $a_1/R = 2.0$, $a_2/R = 0.5$. We first consider the distributions of the physical quantities along a fixed line.

Figures 2(a)–(c) show, respectively, the variations of the stress component σ_{11} (Pa), electric displacement component D_1 ($\times 10^{-9}$ C m^{-2}) and magnetic induction component B_1 ($\times 10^{-7}$ N A^{-1} m^{-1}) along the x_1-axis on the lower interface $x_3 = 0^-$, induced by a uniform dislocation in the x_1-direction with magnitude $d_1 = 0.4$ nm within the elliptical area $S \subset C : 1-(x_1/a_1)^2-(x_2/a_2)^2 = 0$. The ellipse is located horizontally in Material 1 at $x_3/R = h/R = 0.5$. Dislocation with the Burgers vector $\langle 100\rangle$ is often observed in BaTiO$_3$, with magnitude being 0.3992 nm as reported in Lei *et al* (2002) and Sun *et al* (2004).

It can be observed clearly that the distribution of the stress σ_{11} (figure 2(a)) along the x_1-axis is anti-symmetric with respect to $x_1/R = 0$, while the electric displacement D_1 (figure 2(b)) and magnetic induction B_1 (figure 2(c)) are symmetric on two sides of $x_1/R = 0$. Thus the stress σ_{11} is zero at $x_1/R = 0$ (figure 2(a)), whilst the electric displacement D_1 and magnetic induction B_1 both have a local maximum at $x_1/R = 0$. Furthermore, for the size of $(a_1/R, a_2/R) = (0.5, 2.0)$, σ_{11} has a maximum 8.24 Pa at $x_1/R = -0.8$; and for the size of $(a_1/R, a_2/R) = (1.0, 1.0)$, σ_{11} has a maximum 9.64 Pa at $x_1/R = -1.25$. It is interesting that between $x_1/R = -0.4$ and $x_1/R = 0.4$ for the size of $(a_1/R, a_2/R) = (0.5, 2.0)$ and between $x_1/R = -0.8$ and $x_1/R = 0.8$ for the size of $(a_1/R, a_2/R) = (1.0, 1.0)$, σ_{11} shows nearly linear variation (figure 2(a)). For the size of $(a_1/R, a_2/R) = (1.0, 1.0)$, σ_{11} has a local minimum 8.4 Pa at $x_1/R = -0.95$. As for the

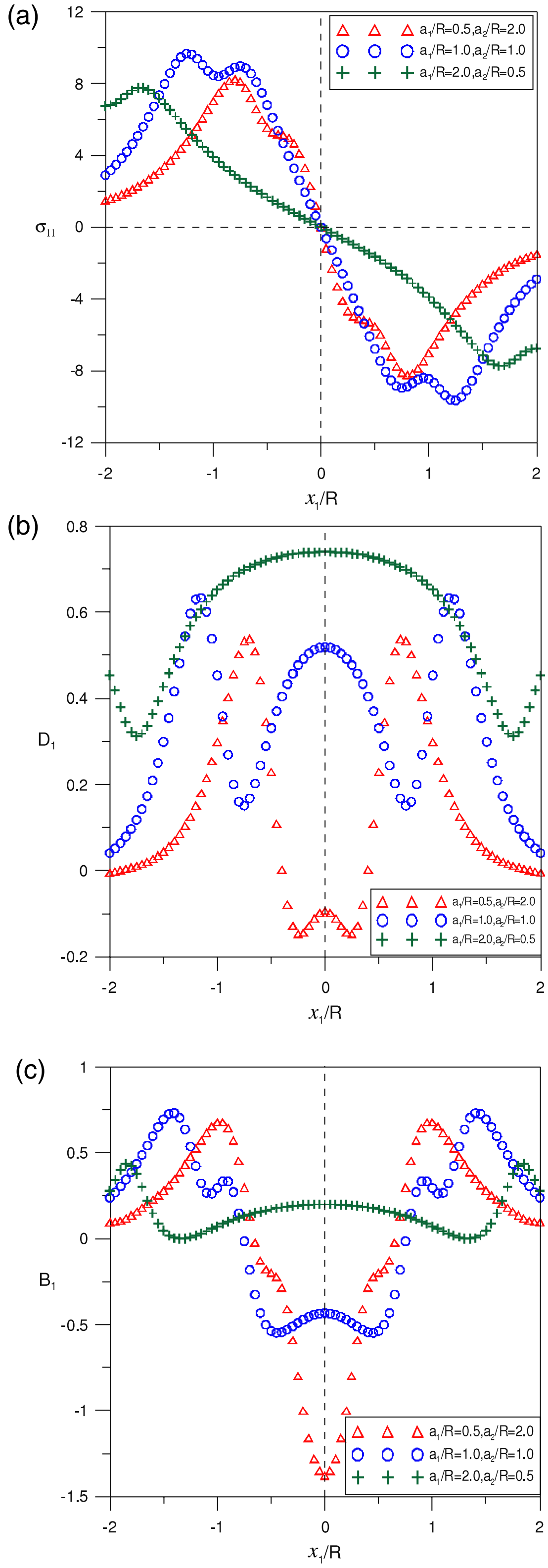

Figure 2. Variation of stress component σ_{11} (Pa) in (a), electric displacement component D_1 ($\times 10^{-9}$ C m^{-2}) in (b), and magnetic induction component B_1 ($\times 10^{-7}$ N A^{-1} m^{-1}) in (c), along line $x_2/R = 0$ on the lower interface $x_3 = 0^-$, induced by a uniform dislocation in the x_1-direction with strength $d_x = d_1 = 0.4$ nm, with the size of the elliptical loading area being $a_1/R = 0.5$, $a_2/R = 2.0$; $a_1/R = 1.0$, $a_2/R = 1.0$; and $a_1/R = 2.0$, $a_2/R = 0.5$. The ellipse is located at $x_3/R = h/R = 0.5$ in Material 1 with center at $(x_1/R, x_2/R) = (0, 0)$.

electric displacement D_1, its value is positive for almost all x_1/R for the sizes of $(a_1/R, a_2/R) = (0.5, 2.0)$ and $(a_1/R, a_2/R) = (1.0, 1.0)$ and also for most x_1/R except for the region near $x_1/R = 0$ for the size of $(a_1/R, a_2/R) = (2.0, 0.5)$ (figure 2(b)). At $x_1/R = 0$, D_1 has a local maximum (figure 2(b)), which is -0.93×10^{-10} C m^{-2}, 0.52×10^{-9} C m^{-2} and 0.74×10^{-9} C m^{-2}, respectively, for the size of $(a_1/R, a_2/R) = (0.5, 2.0)$, $(a_1/R, a_2/R) = (1.0, 1.0)$ and $(a_1/R, a_2/R) = (2.0, 0.5)$. The magnetic induction B_1 is positive near the edge of the ellipse and negative near the center $x_1/R = 0$ (figure 2(c)). For example for the size of $(a_1/R, a_2/R) = (2.0, 0.5)$, B_1 has a minimum -1.38×10^{-7} N A^{-1} m^{-1} at $x_1/R = 0$. In general, from these figures we observe that the higher the ratio a_1/a_2 is, the smoother the variation of the physical quantities along the x_1-axis is.

Figures 3(a)–(c) show, respectively, the variations of stress σ_{11} (Pa), electric displacement D_1 ($\times 10^{-12}$ C m^{-2}) and magnetic induction B_1 ($\times 10^{-10}$ N A^{-1} m^{-1}) along the x_1-axis on the lower interface $x_3 = 0^-$, induced by a uniform traction in the x_1-direction with magnitude $t_1 = 1$ Pa within the elliptical area $S \subset C : 1 - (x_1/a_1)^2 - (x_2/a_2)^2 = 0$ located in Material 1 at $x_3/R = 0.5$. Compared to those due to the uniform dislocation in figure 2, we observe that while their symmetry features are the same, the response curve induced by the uniform traction is much smoother than the corresponding curve due to the uniform dislocation. For instance, the distribution of stress σ_{11} (figure 3(a)) is anti-symmetric with respect to $x_1/R = 0$, whilst electric displacement D_1 (figure 3(b)) and magnetic induction B_1 (figure 3(c)) are symmetric about $x_1/R = 0$. For the size of $(a_1/R, a_2/R) = (0.5, 2.0)$, stress σ_{11} has a maximum 0.173 Pa at $x_1/R = -0.9$; for the size of $(a_1/R, a_2/R) = (1.0, 1.0)$, the maximum σ_{11} occurs at $x_1/R = -1.2$ with a value of 0.213 Pa; for the size of $(a_1/R, a_2/R) = (2.0, 0.5)$, the maximum value of σ_{11} is 0.19 Pa located at $x_1/R = -1.85$ (figure 3(a)). As for D_1, it has only one maximum located at the center $x_1/R = 0$ (figure 3(b)), and on both sides of $x_1/R = 0$ it decreases monotonically. The maximum values of D_1 for the sizes $(a_1/R, a_2/R) = (0.5, 2.0)$, $(a_1/R, a_2/R) = (1.0, 1.0)$ and $(a_1/R, a_2/R) = (2.0, 0.5)$ are correspondingly 22.4×10^{-12} C m^{-2}, 32.0×10^{-12} C m^{-2} and 29.7×10^{-12} C m^{-2} (figure 3(b)). It is interesting to point out that the maximum value of D_1 for the size of $(a_1/R, a_2/R) = (1.0, 1.0)$ (i.e., for the circular loading case) is the largest among all. The curves for B_1 show some fluctuation, which is similar to that under the dislocation loading (figure 3(c)). At $x_1/R = 0$, the minimum value of B_1 is zero for the size of $(a_1/R, a_2/R) = (1.0, 1.0)$ and -10.2×10^{-10} N A^{-1} m^{-1} for the size of $(a_1/R, a_2/R) = (2.0, 0.5)$.

5.2. Effect of material anisotropy

In the previous example, we have assumed that the symmetry axis of the material is along the x_3-axis. It is well known that material orientation relative to the interface can greatly influence the induced field. Thus, in the second example,

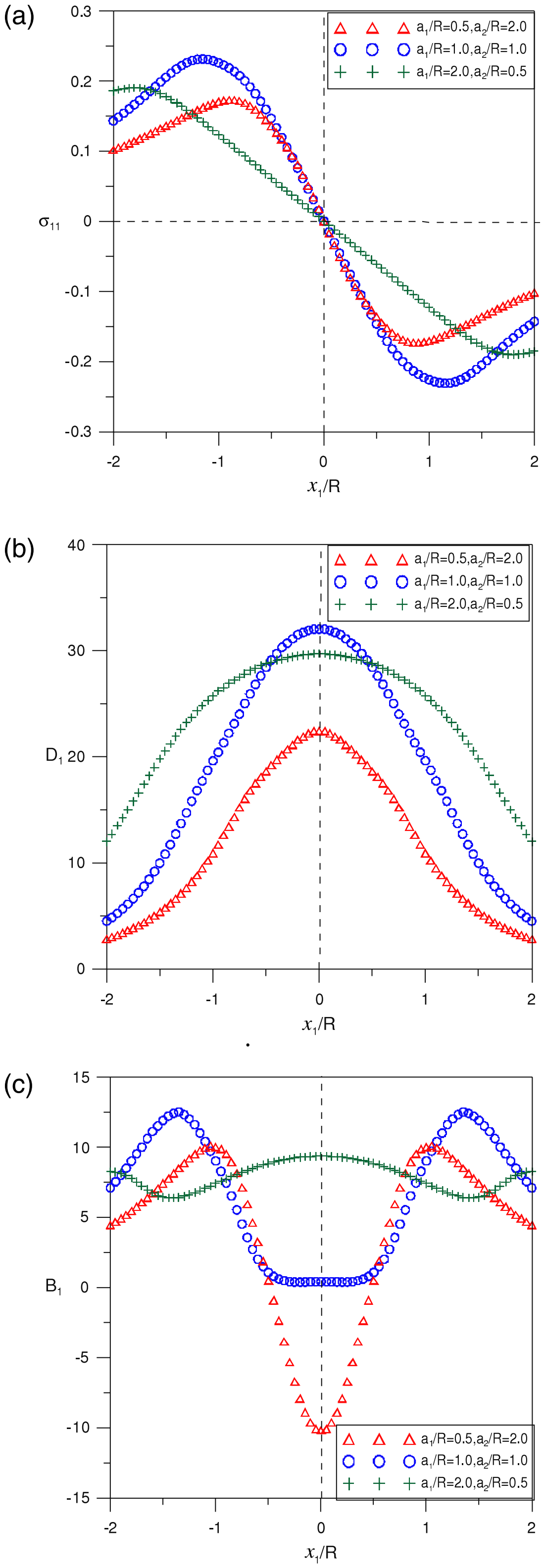

Figure 3. Variation of stress component σ_{11} (Pa) in (a), electric displacement component D_1 ($\times 10^{-12}$ C m^{-2}) in (b), and magnetic induction component B_1 ($\times 10^{-10}$ N A^{-1} m^{-1}) in (c), along line $x_2/R = 0$ on the lower interface $x_3 = 0^-$, induced by a uniform traction in x_1-direction with strength $t_x = t_1 = 1$ Pa, with the size of the elliptical loading area being $a_1/R = 0.5$, $a_2/R = 2.0$; $a_1/R = 1.0$, $a_2/R = 1.0$; and $a_1/R = 2.0$, $a_2/R = 0.5$. The ellipse is located at $x_3/R = h/R = 0.5$ in Material 1 with center at $(x_1/R, x_2/R) = (0, 0)$.

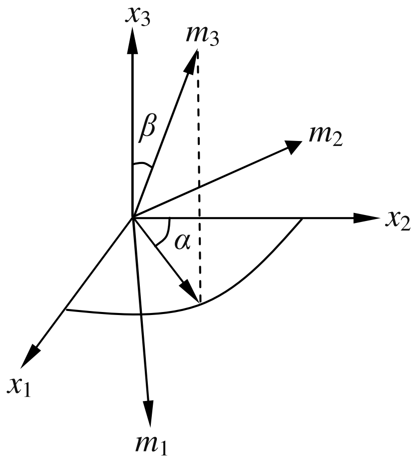

Figure 4. Relation between the material coordinates (m_1, m_2, m_3) and the global coordinates (x_1, x_2, x_3) determined by the rotation angles α and β. The material axes coincide with the global axes when $\alpha = 90°$, $\beta = 0°$.

we will numerically investigate the effect of the material orientation on the induced field, including stress, electric displacement and magnetic induction. We still use the pseudo-$BaTiO_3$ for the upper half-space. For the lower half-space, however, we rotate the MEE composite of 50% $BaTiO_3$ and 50% $CoFe_2O_4$ using the transformation shown in figure 4 where (m_1, m_2, m_3) denotes the transversely isotropic material coordinate system (with m_3 being the axis of symmetry) and (x_1, x_2, x_3) the global coordinate system used in the paper. The general relationship between the two coordinate systems is

$$\begin{bmatrix} x_1 \\ x_2 \\ x_3 \end{bmatrix} = \begin{bmatrix} \sin\alpha\cos\beta & \cos\alpha & -\sin\alpha\sin\beta \\ -\cos\alpha\cos\beta & \sin\alpha & \cos\alpha\sin\beta \\ \sin\beta & 0 & \cos\beta \end{bmatrix} \begin{bmatrix} m_1 \\ m_2 \\ m_3 \end{bmatrix}, \tag{55}$$

where α and β are the two rotation angles shown in figure 4.

The original material orientation, which coincides with the global coordinate directions, based on equation (55), is at $\alpha = 90°$, $\beta = 0°$. The material properties in the lower half-space after rotation with $\alpha = 0°$, $\beta = 90°$ can be found in the appendix B.

Figures 5–10 show the contours of some physical quantities (on the interface or the lower side of the interface) induced by the uniform electric potential dislocation (or jump) ϕ with strength 1 V within an ellipse (a) before and (b) after coordinate transformation. The ellipse with fixed semi-axes $a_1/R = 2.0$, $a_2/R = 1.0$ is horizontally located at $x_3/R = h/R = 0.5$ in Material 1 centered at $(x_1/R, x_2/R) = (0, 0)$. Table 1 lists the maximum and minimum values of the physical quantities shown in figures 5–10. Among all these quantities, stress σ_{11}

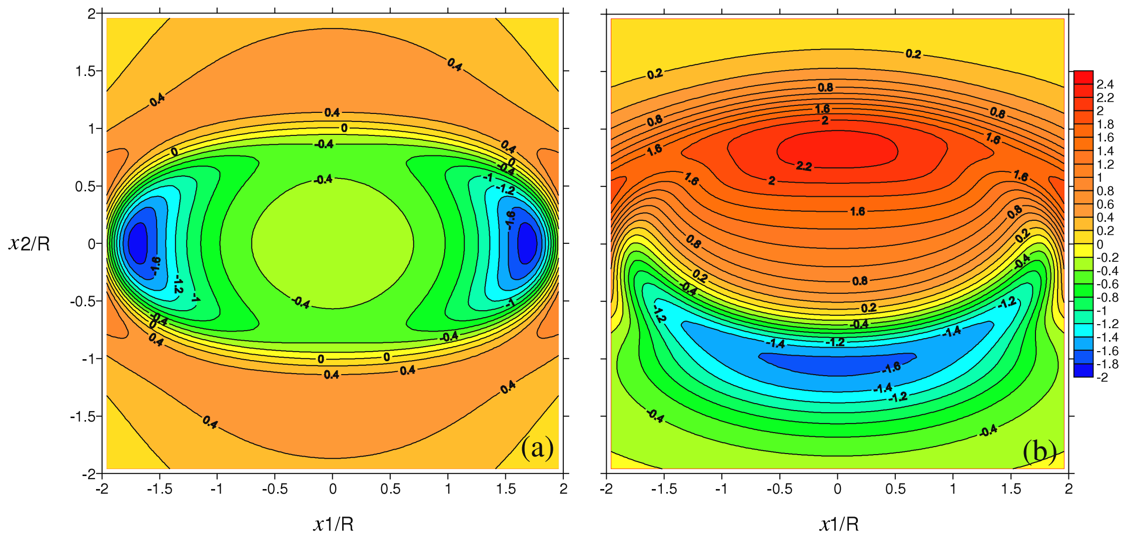

Figure 5. Contours of stress component σ_{11} (Pa) on lower interface $x_3 = 0^-$ before coordinate rotation in (a) and after coordinate rotation ($\alpha = 0°$, $\beta = 90°$) in (b), induced by an electric potential jump with strength $\Delta\phi = 1$ V in the elliptical area of $a_1/R = 2.0$, $a_2/R = 1.0$ located at $x_3/R = h/R = 0.5$ in Material 1 centered at $(x_1/R, x_2/R) = (0, 0)$.

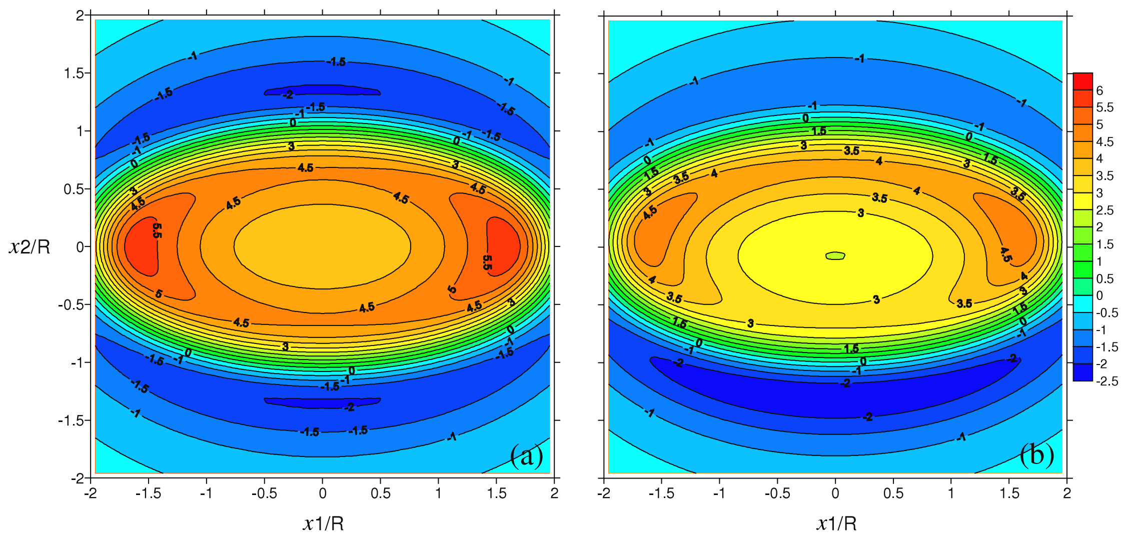

Figure 6. Contours of stress component σ_{33} (Pa) on interface $x_3 = 0$ before coordinate rotation in (a) and after coordinate rotation ($\alpha = 0°$, $\beta = 90°$) in (b), induced by an electric potential jump with strength $\Delta\phi = 1$ V in the elliptical area of $a_1/R = 2.0$, $a_2/R = 1.0$ located at $x_3/R = h/R = 0.5$ in Material 1 centered at $(x_1/R, x_2/R) = (0, 0)$.

Table 1. Maximum and minimum values of different physical quantities induced by a uniform electric potential dislocation (or jump) $\Delta\phi = 1$ V within an ellipse before ($\alpha = 90°$, $\beta = 0°$) and after ($\alpha = 0°$, $\beta = 90°$) coordinate transformation. The ellipse has fixed major and minor axes $a_1/R = 2.0$, $a_2/R = 1.0$ located at $x_3/R = h/R = 0.5$ in Material 1 centered at $(x_1/R, x_2/R) = (0, 0)$.

		σ_{11} (Pa)	σ_{33} (Pa)	D_1 (10^{-9} C m^{-2})	D_3 (10^{-9} C m^{-2})	B_1 (10^{-8} T)	B_3 (10^{-8} T)
$\alpha = 90°$, $\beta = 0°$	Max	0.79	5.81	2.02	0.47	2.85	2.31
	Min	−1.9	−2.03	−2.02	−2.72	−2.85	−0.98
$\alpha = 0°$, $\beta = 90°$	Max	2.29	4.91	2.23	0.63	1.69	1.6
	Min	−1.65	−2.43	−2.23	−2.99	−1.69	−0.9

is the most influenced. For example, its contour shapes after the coordinate transformation (figure 5(b)) are completely different to the ones before the coordinate transformation (figure 5(a)). We further see from table 1 that the maximum values of σ_{11} and B_1 after the coordinate transformation are almost three times larger than the ones before the coordinate

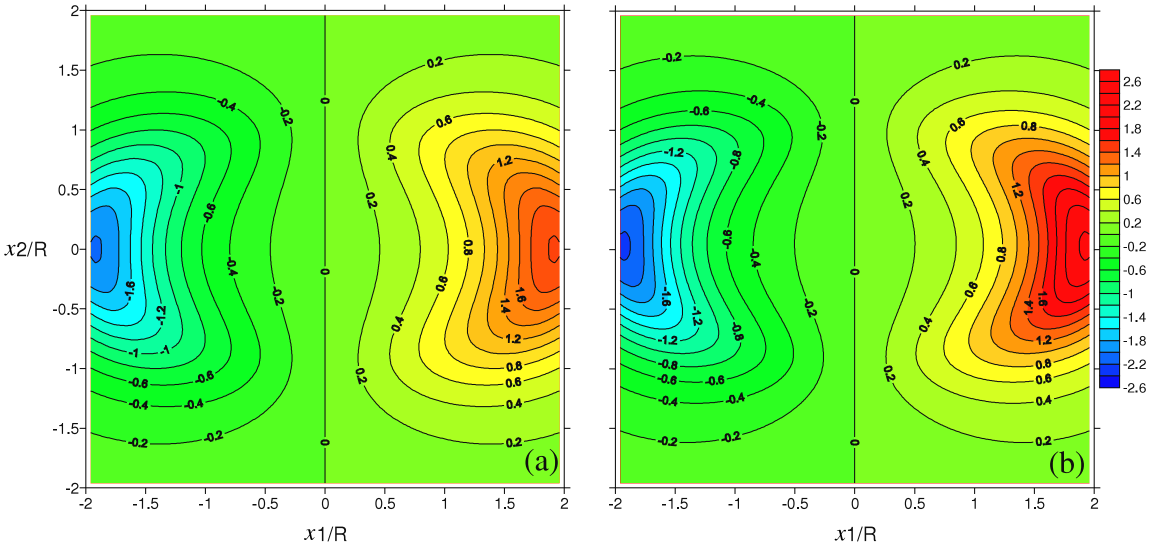

Figure 7. Contours of electric displacement component D_1 ($\times 10^{-9}$ C m^{-2}) on lower interface $x_3 = 0^-$ before coordinate rotation in (a) and after coordinate rotation ($\alpha = 0°$, $\beta = 90°$) in (b), induced by an electric potential jump with strength $\Delta\phi = 1$ V in the elliptical area of $a_1/R = 2.0$, $a_2/R = 1.0$ located at $x_3/R = h/R = 0.5$ in Material 1 centered at $(x_1/R, x_2/R) = (0, 0)$.

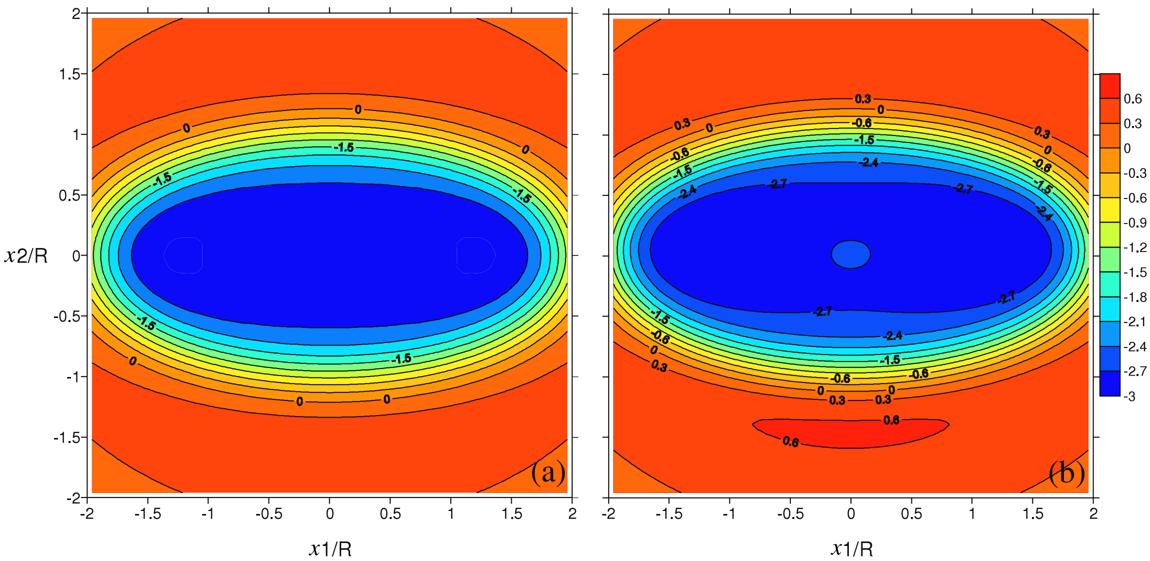

Figure 8. Contours of electric displacement component D_3 ($\times 10^{-9}$ C m^{-2}) on interface $x_3 = 0$ before coordinate rotation in (a) and after coordinate rotation ($\alpha = 0°$, $\beta = 90°$) in (b), induced by an electric potential jump with strength $\Delta\phi = 1$ V in the elliptical area of $a_1/R = 2.0$, $a_2/R = 1.0$ located at $x_3/R = h/R = 0.5$ in Material 1 centered at $(x_1/R, x_2/R) = (0, 0)$.

transformation. It is also observed that before and after the coordinate transformation, the distributions of D_1 and B_1 are always anti-symmetric with respect to $x_1/R = 0$.

6. Conclusions

We have derived an analytical solution for a magnetoelectroelastic bimaterial system under the action of extended traction and dislocation uniformly distributed over a horizontal ellipse. The solution is obtained by making use of two-dimensional Fourier transformation combined with the Stroh formalism. In dealing with the elliptical shape, a simple scale transformation technique is also applied to the two horizontal variables both in the physical and transformed domains. The solution is very general and contains various decoupled material systems and reduced material domains (infinite and half-space) as special cases.

As numerical examples, an MEE bimaterial system made of $BaTiO_3/CoFe_2O_4$ is investigated under both traction and dislocation loads within an elliptical area with various semi-axes ratios. It is observed that: (1) the induced field due to traction is smoother than that due to the dislocation; (2) different elliptical semi-axes ratios can significantly influence the induced elastic, electric and magnetic fields; (3) material orientation (relative to the interface) can also remarkably influence the induced fields.

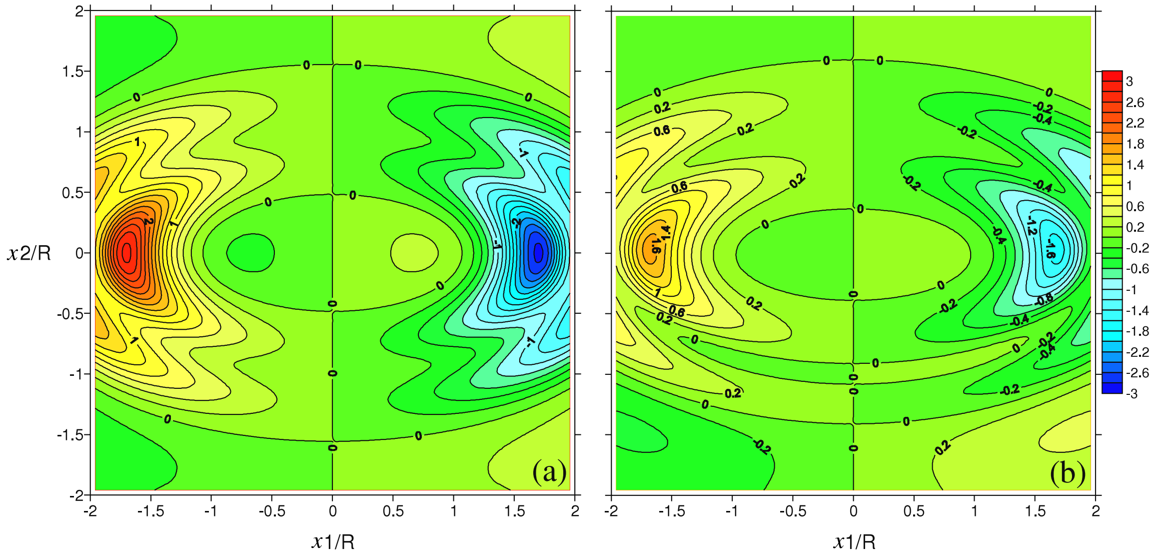

Figure 9. Contours of magnetic induction component B_1 ($\times 10^{-8}$ T) on lower interface $x_3 = 0^-$ before coordinate rotation in (a) and after coordinate rotation ($\alpha = 0°$, $\beta = 90°$) in (b), induced by an electric potential jump with strength $\Delta\phi = 1$ V in the elliptical area of $a_1/R = 2.0$, $a_2/R = 1.0$ located at $x_3/R = h/R = 0.5$ in Material 1 centered at $(x_1/R, x_2/R) = (0, 0)$.

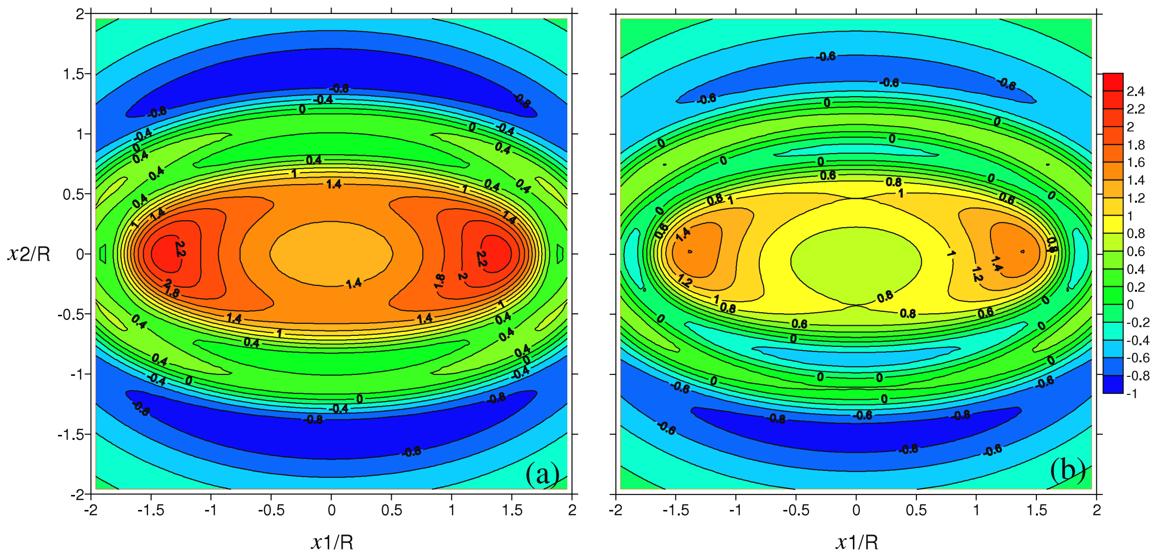

Figure 10. Contours of magnetic induction component B_3 ($\times 10^{-8}$ T) on interface $x_3 = 0$ before coordinate rotation in (a) and after coordinate rotation ($\alpha = 0°$, $\beta = 90°$) in (b), induced by an electric potential jump with strength $\Delta\phi = 1$ V in the elliptical area of $a_1/R = 2.0$, $a_2/R = 1.0$ located at $x_3/R = h/R = 0.5$ in Material 1 centered at $(x_1/R, x_2/R) = (0, 0)$.

Acknowledgments

The first author would like to acknowledge the support of the Shanghai Eastern Scholar Plan in Shanghai Institutes and of the State Key Laboratory of Mechanical Behavior of Materials.

Appendix A

The derivation of the compact form of the fundamental equations for MEE material is presented in this appendix for easy reference.

For a static problem, the field equations for a linear, anisotropic magnetoelectroelastic solid are as follows.

(i) Equilibrium equations (including the force balance, electric and magnetic balances):

$$\begin{aligned} \sigma_{ij,j} + f_i &= 0, \\ D_{i,i} &= f_e, \\ B_{i,i} &= f_m, \end{aligned} \tag{A.1}$$

where σ_{ij}, D_i and B_i are the stress, electric displacement and magnetic induction, respectively; f_i, f_e and f_m are the body force, electric, and magnetic charges, respectively; A subscript comma denotes the partial derivative with respect to the coordinate.

(ii) Constitutive relations:

$$\begin{aligned} \sigma_{ij} &= c_{ijlm}\gamma_{lm} - e_{kji}E_k - q_{kji}H_k, \\ D_i &= e_{ijk}\gamma_{jk} + \varepsilon_{ij}E_j + \alpha_{ij}H_j, \\ B_i &= q_{ijk}\gamma_{jk} + \alpha_{ji}E_j + \mu_{ij}H_j, \end{aligned} \tag{A.2}$$

where γ_{ij}, E_i and H_i are the strain, electric and magnetic fields, respectively; c_{ijlm}, e_{ijk}, q_{ijk} and α_{ij} are the elastic, piezoelectric, piezomagnetic and magnetoelectric coefficients, respectively; ε_{ij} and μ_{ij} are the dielectric permittivities and magnetic permeabilities, respectively.

(iii) Strain–displacement, electric field–electric potential and magnetic field–magnetic potential relations:

$$\begin{aligned} \gamma_{ij} &= \tfrac{1}{2}(u_{i,j} + u_{j,i}), \\ E_i &= -\phi_{,i}, \\ H_i &= -\psi_{,i}, \end{aligned} \tag{A.3}$$

where u_i, ϕ and ψ are the elastic displacement, electric and magnetic potentials, respectively.

Utilizing the short notation introduced by Pan (2002), the extended quantities for the displacement, stress, strain, material coefficient, and body force in magnetoelectroelastic media can be expressed, respectively, as

$$u_I = \begin{cases} u_i & I = i = 1, 2, 3; \\ \phi & I = 4; \\ \psi & I = 5; \end{cases} \tag{A.4}$$

$$\sigma_{iJ} = \begin{cases} \sigma_{ij} & J = j = 1, 2, 3; \\ D_i & J = 4; \\ B_i & J = 5; \end{cases} \tag{A.5}$$

$$\gamma_{Ij} = \begin{cases} \gamma_{ij} & I = i = 1, 2, 3 \\ -E_j & I = 4; \\ -H_j & I = 5; \end{cases} \tag{A.6}$$

$$c_{iJKl} = \begin{cases} c_{ijkl} & J, K = j,\ k = 1, 2, 3; \\ e_{lij} & J = j = 1, 2, 3;\ K = 4; \\ e_{ikl} & J = 4;\ K = k = 1, 2, 3; \\ q_{lij} & J = j = 1, 2, 3;\ K = 5; \\ q_{ikl} & J = 5;\ K = k = 1, 2, 3; \\ -\alpha_{il} & J = 4,\ K = 5 \text{ or } K = 4, J = 5; \\ -\varepsilon_{il} & J, K = 4; \\ -\mu_{il} & J, K = 5; \end{cases} \tag{A.7}$$

$$f_J = \begin{cases} f_i & J = j = 1, 2, 3; \\ -f_e & J = 4; \\ -f_m & J = 5. \end{cases} \tag{A.8}$$

Thus, in terms of the short notation in equations (A.4)–(A.8), the equilibrium equations (A.1) can be recast into

$$\sigma_{iJ,i} + f_J = 0 \tag{A.9}$$

and the constitutive relations (A.2) can be unified into a single one as

$$\sigma_{iJ} = c_{iJKl}u_{K,l}. \tag{A.10}$$

Appendix B

The global material constants of MEE composite of 50% $BaTiO_3$ and 50% $CoFe_2O_4$ after rotation ($\alpha = 0°$, $\beta = 90°$) are presented below.

(1) Elastic constants

$$[c] = \begin{bmatrix} 225 & 124 & 125 & 0.0 & 0.0 & 0.0 \\ & 216 & 124 & 0.0 & 0.0 & 0.0 \\ & & 225 & 0.0 & 0.0 & 0.0 \\ & & & 44.0 & 0.0 & 0.0 \\ & \text{symm.} & & & 50.0 & 0.0 \\ & & & & & 44.0 \end{bmatrix} (10^9\ \mathrm{N\ m^{-2}}).$$

(2) Piezoelectric constants

$$[e] = \begin{bmatrix} 0.0 & 0.0 & 0.0 & 0.0 & 0.0 & 5.8 \\ -2.2 & 9.3 & -2.2 & 0.0 & 0.0 & 0.0 \\ 0.0 & 0.0 & 0.0 & 5.8 & 0.0 & 0.0 \end{bmatrix} (\mathrm{C\ m^{-2}}).$$

(3) Dielectric permeability coefficients

$$[\varepsilon] = \begin{bmatrix} 5.64 & 0.0 & 0.0 \\ 0.0 & 6.35 & 0.0 \\ 0.0 & 0.0 & 5.64 \end{bmatrix} (10^{-9}\ \mathrm{C\ V^{-1}\ m^{-1}}).$$

(4) Piezomagnetic constants

$$[\beta] = \begin{bmatrix} 0.0 & 0.0 & 0.0 & 0.0 & 0.0 & 275.0 \\ 290.2 & 350 & 290.2 & 0.0 & 0.0 & 0.0 \\ 0.0 & 0.0 & 0.0 & 275 & 0.0 & 0.0 \end{bmatrix} (\mathrm{N\ A^{-1}\ m^{-1}}).$$

(5) Magnetoelectric coefficients $\alpha(i, j) = 0$ (for $i, j = 1, 3$) (in $\mathrm{N\ s\ V^{-1}\ C^{-1}}$).

(6) Magnetic permeability coefficients

$$[\mu] = \begin{bmatrix} 297 & 0.0 & 0.0 \\ 0.0 & 83.5 & 0.0 \\ 0.0 & 0.0 & 297 \end{bmatrix} (10^{-6}\ \mathrm{N\ s^2\ C^{-2}}).$$

References

Barnett D M and Lothe J 1975 Dislocations and line charges in anisotropic piezoelectric insulators *Phys. Status Solidi* b **67** 105–11

Chu H J, Zhang Y, Pan E and Han Q K 2011 Circular surface loading on a layered multiferroic half space *Smart Mater. Struct.* **20** 035020

Deresiewicz H 1960 The half-space under pressure distributed over an elliptical portion of its plane boundary *J. Appl. Mech.* **27** 111–9

Ding H J, Jiang A M, Hou P F and Chen W Q 2005 Green's functions for two-phase transversely isotropic magneto-electro-elastic media *Eng. Anal. Bound. Elem.* **29** 551–61

Eerenstein W, Mathur N D and Scott J F 2006 Multiferroic and magnetoelectric materials *Nature* **442** 759–65

Lei C H, Van Tendeloo G, Siegert M and Schubert J 2002 Microstructural investigation of $BaTiO_3$ thin films deposited on (001) MgO *J. Mater. Res.* **17** 1923–31

Liu J X, Liu X L and Zhao Y B 2001 Green's functions for anisotropic magnetoelectroelastic solids with an elliptical cavity or a crack *Int. J. Eng. Sci.* **39** 1405–18

Ma J, Hu J, Li Z and Nan C W 2011 Recent progress in multiferroic magnetoelectric composites: from bulk to thin films *Adv. Mater.* **23** 1062–87

Pan E 2002 Three-dimensional Green's functions in anisotropic magneto-electro-elastic bimaterials *Z. Angew. Math. Phys.* **53** 815–38

Pan E and Yuan F G 2000 Three-dimensional Green's functions in anisotropic bimaterials *Int. J. Solids Struct.* **37** 5329–51

Ryu J, Priya S, Uchino K and Kim H 2002 Magnetoelectric effect in composites of magnetostrictive and piezoelectric materials *J. Electroceram.* **8** 107–19

Sun H P, Tian W, Pan X Q, Haeni J H and Schlom D G 2004 Evolution of dislocation arrays in epitaxial $BaTiO_3$ thin films grown on (100) $SrTiO_3$ *Appl. Phys. Lett.* **84** 3298

Ting T C T 1996 *Anisotropic Elasticity: Theory and Applications* (New York: Oxford University Press)

Wang X and Pan E 2008 Two-dimensional Green's functions in anisotropic multiferroic bimaterials with a viscous interface *J. Mech. Phys. Solids* **56** 2863–75

Wang X, Pan E, Albrecht J D and Feng W J 2009 Effective properties of multilayered functionally graded multiferroic composites *Compos. Struct.* **87** 206–14

Wang H M, Pan E, Sangghaleh A, Wang R and Han X 2012 Circular loadings on the surface of an anisotropic and magnetoelectroelastic half-space *Smart Mater. Struct.* **21** 075003

Watson G N 1966 *A Treatise on the Theory of Bessel Functions* 2nd edn (Cambridge: Cambridge University Press)

Willis J R 1966 Hertzian contact of anisotropic bodies *J. Mech. Phys. Solids* **14** 163–76

Xue C X, Pan E and Zhang S Y 2011 Solitary waves in a magnetoelectro-elastic circular rod *Smart Mater. Struct.* **20** 105010

Zhao Y F, Shang X C and Pan E 2013 Analytical solutions of uniform extended dislocations and tractions over a circular area in anisotropic magnetoelectroelastic bimaterials *Acta Mech. Sin.* **29** 73–84